Modeled Streamflow Response to Scenarios of Tundra Lake Water Withdrawal and Seasonal Climate Extremes, Arctic Coastal Plain, Alaska

Anne Gädeke[1,2] [ID], **Christopher D. Arp[1]** [ID], **Anna K. Liljedahl[1,3]** [ID], **Ronald P. Daanen[4]**, **Lei Cai[5,6]** [ID], **Vladimir A. Alexeev[5]** [ID], **Benjamin M. Jones[1]**, **Mark S. Wipfli[7]** [ID], and **Jörg Schulla[8]**

[1]Water and Environmental Research Center, University of Alaska Fairbanks, Fairbanks, AK, USA, [2]Potsdam Institute for Climate Impact Research, Potsdam, Germany, [3]Woodwell Climate Research Center, Falmouth, MA, USA, [4]Alaska Department of Natural Resources, Division of Geological and Geophysical Surveys, Fairbanks, AK, USA, [5]International Arctic Research Center, University of Alaska Fairbanks, Fairbanks, AK, USA, [6]Department of Atmospheric Sciences, Yunnan University, Kunming, Yunnan, China, [7]U.S. Geological Survey, Alaska Cooperative Fish and Wildlife Research Unit, Institute of Arctic Biology, University of Alaska Fairbanks, Fairbanks, AK, USA, [8]Hydrology Software Consulting, Zurich, Switzerland

Abstract On the Arctic Coastal Plain (ACP) in northern Alaska (USA), permafrost and abundant surface-water storage define watershed hydrological processes. In the last decades, the ACP landscape experienced extreme climate events and increased lake water withdrawal (LWW) for infrastructure construction, primarily ice roads and industrial operations. However, their potential (combined) effects on streamflow are relatively underexplored. Here, we applied the process-based, spatially distributed hydrological and thermal Water Balance Simulation Model (10 m spatial resolution) to the 30 km² Crea Creek watershed located on the ACP. The impacts of documented seasonal climate extremes and LWW were evaluated on seasonal runoff (May–August), including minimum 7-day mean flow (MQ7), the recovery time of MQ7 to pre-perturbation conditions, and the duration of streamflow conditions that prevents fish passage. Low-rainfall scenarios (21% of normal, one to three summers in a row) caused a larger reduction in MQ7 (−56% to −69%) than LWW alone (−44% to −58%). Decadal-long consecutive LWW under average climate conditions resulted in a new equilibrium in low flow and seasonal runoff after 3 years that included a disconnected stream network, a reduced watershed contributing area (54% of total watershed area), and limited fish passage of 20 days (vs. 6 days under control conditions) throughout summer. Our results highlight that, even under current average climatic conditions, LWW is not offset by same-year snowmelt as currently assumed in land management regulations. Effective land management would therefore benefit from considering the combined impact of climate change and industrial LWWs.

1. Introduction

Watersheds on the Arctic Coastal Plain (ACP) in northern Alaska are constrained near or at the surface as the presence of deep (100–600 m) permafrost and a shallow (<1 m) active layer (the seasonally thawed surface layer above permafrost; Jorgenson et al., 2014) inhibit deep percolation and encourage immediate runoff (Woo, 1986). During short Arctic summers, expansive but intermittently connected surface drainage networks, mosaics of lakes, ponds, and wetlands set in the ice-wedge polygonized tundra characterize the landscape. Surface water connectivity, the flow between two unique landscape elements such as a lake and a larger stream linked by a stream channel, controls freshwater habitat availability and movement of locally migrating and dispersing fish (Heim et al., 2016; Laske et al., 2016). The seasonality of snowmelt, rainfall, and evapotranspiration govern the connectivity (Bowling et al., 2003; Lesack & Marsh, 2010) among lakes, ponds, and wetlands. Surface water connectivity is at its seasonal maximum at the end of the snowmelt (Bowling et al., 2003) allowing fish to move from overwintering to summer spawning and foraging habitats (Heim et al., 2016). Runoff and surface water inundation gradually decline up through mid-summer, leading to a fragmentation of drainage networks (Bowling et al., 2003). Lowest flows typically occur in early fall (September–October) just prior to freeze-up at a time when fish migrate to overwintering habitats (Arp, Whitman, et al., 2012). Recent studies show that the ACP hydrologic regime has become subject to greater interannual discharge variability (Stuefer et al., 2017) which

Methodology: Anne Gädeke, Christopher D. Arp, Anna K. Liljedahl, Ronald P. Daanen, Benjamin M. Jones

Project Administration: Christopher D. Arp

Resources: Anna K. Liljedahl, Lei Cai, Vladimir A. Alexeev

Software: Anne Gädeke, Ronald P. Daanen, Jörg Schulla

Supervision: Christopher D. Arp, Anna K. Liljedahl, Ronald P. Daanen

Validation: Anne Gädeke, Jörg Schulla

Visualization: Anne Gädeke

Writing – original draft: Anne Gädeke

Writing – review & editing: Anne Gädeke, Christopher D. Arp, Anna K. Liljedahl, Ronald P. Daanen, Lei Cai, Vladimir A. Alexeev, Benjamin M. Jones, Jörg Schulla

can primarily be attributed to increased variability in precipitation amounts and type as year-to-year variability in total evapotranspiration is relatively small (Liljedahl et al., 2017). A larger variability in runoff may increase uncertainty in surface water connectivity (Betts & Kane, 2015; Lesack & Marsh, 2010) and can therefore alter patterns of fish migration (Heim et al., 2016) and fish populations (Heim et al., 2019).

The ACP is currently experiencing environmental change that may modify hydrologic processes from local to regional scales. The Arctic has experienced amplified climate warming since the 1970s (Serreze & Francis, 2006), which directly and indirectly affects hydrologic systems. Degrading permafrost (Jorgenson et al., 2006) deepening of the active layer (Oelke et al., 2004), and thermokarst erosion (Jones et al., 2011) can alter hydrologic storage and flow paths resulting in new runoff regimes (Liljedahl et al., 2016). Climate warming has also been associated with increasing rates and variability of precipitation amount and type, evapotranspiration, and runoff (Déry et al., 2009; Stuefer et al., 2017), often referred to as hydrological intensification (Arp, Whitman, et al., 2020; Rawlins et al., 2010). Earlier lake ice-out has been estimated to increase lake evaporation (Arp, Jones, et al., 2015), which in turn may suppress summer runoff in lake-dominated watersheds (Arp, Whitman, et al., 2012; Bowling et al., 2003). The most extreme low rainfall (LR) summer in recent history on Alaska's North Slope was in 2007, which presented the second lowest rainfall in the 1949–2014 period (Liljedahl et al., 2017) and that contributed to a large tundra fire (Jones et al., 2015) and extreme low soil moisture (Liljedahl et al., 2011) and runoff in ACP rivers (Arp, Whitman, et al., 2012; Stuefer et al., 2017).

Land-use changes in the ACP are primarily associated with natural resource extraction and associated infrastructure. Oil and gas exploration in the National Petroleum Reserve Alaska (NPR-A) relies heavily on freshwater resources to build winter ice roads. Most of this water comes from abundant and widely distributed lakes on the ACP. Lakes with depths exceeding maximum ice thickness (floating-ice lakes) are the main water source, while also serving as overwintering fish habitats (Jones et al., 2009). Currently, management of industrial lake water-use is based primarily on consideration of overwintering fish habitat and regulations assume that pumped lakes are (a) fully recharged during the subsequent snowmelt and (b) that there is minimal impact on summer surface water connectivity to downstream habitats (i.e., streamflow). However, studies have shown that lakes are a main source in maintaining streamflow in summer (Arp, Whitman, et al., 2012, 2015). We hypothesized that winter lake water withdrawal (LWW) lowers runoff not only during the snowmelt peak event, but also throughout the summer, and potentially for multiple subsequent summers. The impact of LWW on the following summer's downstream flows has only recently been considered by policy makers.

Land managers of the NPR-A are increasingly concerned and wish to understand potential impacts of increased climatic variability and LWW on watershed hydrology and habitat connectivity, especially how it may affect fish populations (Arp et al., 2019). Therefore, our objectives were to refine our understanding of hydrologic responses both in terms of magnitude (focus on low flows), timing, duration, and recovery time to scenarios of (a) observed seasonal climate extremes, (b) documented industrial LWW and (c) a combination thereof by applying the Water Balance Simulation Model (WaSiM) to the 30 km² Crea Creek watershed located in the NPR-A. Crea Creek is representative of many ACP watersheds due to its seasonally flowing low-gradient beaded stream systems, and abundance of vegetated drained thermokarst lake basins (Arp, Whitman, et al., 2015). Our findings may support decision makers to craft informed management plans, which can guide conservation, subsistence, and industry needs, within the ACP and beyond in similar Arctic tundra environments.

2. Study Area

Our study focused on the Crea Creek watershed (30 km²), a sub-watershed of the Fish Creek drainage system (4,600 km², Figure 1). Crea Creek watershed is located within the northeast portion of the NPR-A, approximately halfway between Prudhoe Bay and Utqiaġvik (formerly Barrow), on the ACP of northern Alaska. The watershed is underlain by continuous permafrost, reaching depths of 270 m (Clow, 2014). Taliks, unfrozen soils within permafrost, occur under lakes and rivers (Jorgenson et al., 2014) and the active layer is shallow ranging between 30 and 60 cm. Marine sand and silt represent the dominant surficial geology. Vegetation consists primarily of sedges (*Carex* spp.) in drained thermokarst lake basins (DTLBs) and low-centered ice-wedge polygons. Cotton grasses (*Eriophorum* spp.) cover upland tussock tundra and mosaics of sedges, willows (*Salix* spp.), and dwarf birch (*Betula nana*) occur in riparian zones. Long, cold winters and short, cool summers with low precipitation,
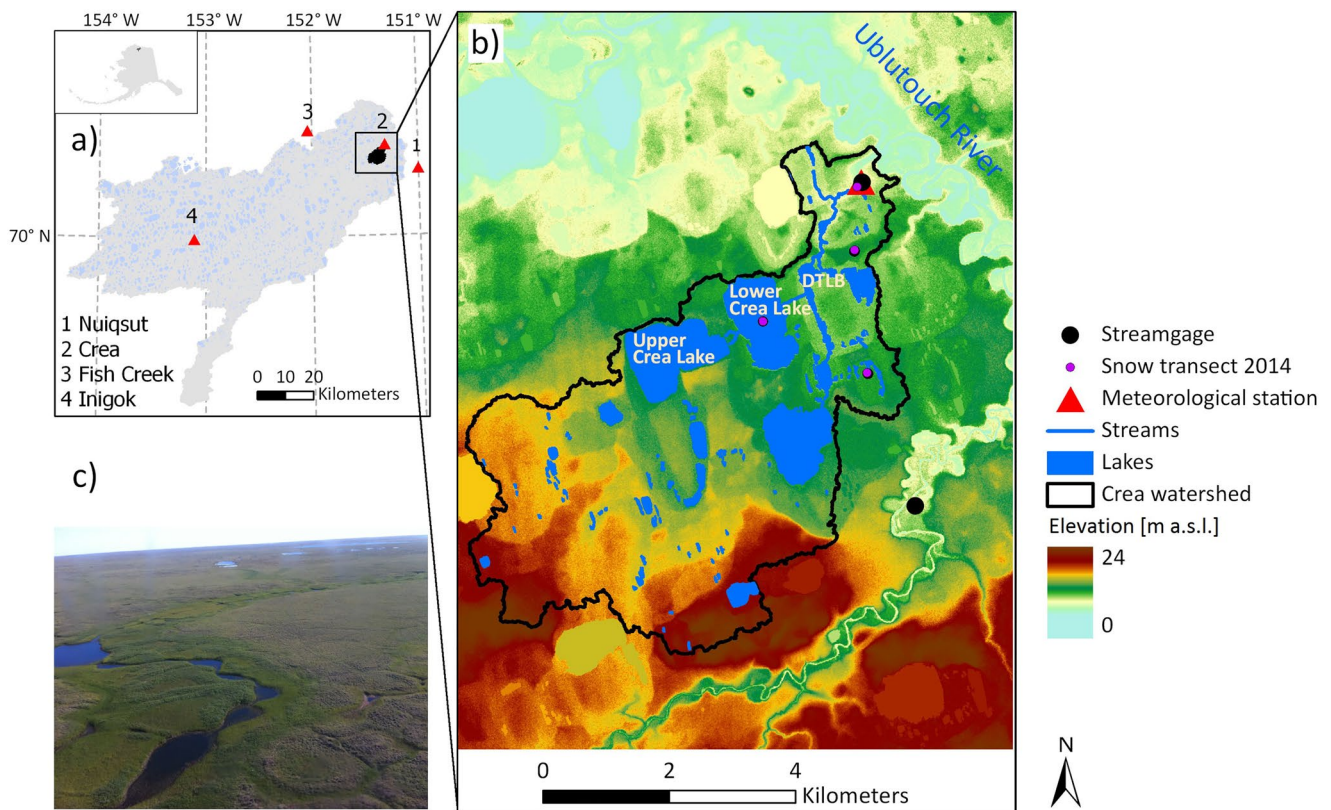
Figure 1. Location of Crea Creek watershed (subwatershed of Fish Creek on the Arctic Coastal Plain [Alaska, USA]), including meteorological stations (a). Elevation and location of field measurements, Upper Crea Lake, Lower Crea Lake, and drained thermokarst lake basin (DTLB) in Crea Creek watershed (b). Aerial photo (c) showing the beaded stream of Crea Creek close to its outlet (1 August 2015).

characterize much of the ACP. At Fish Creek station (Figure 1, Table 1), mean annual air temperature is −10.7°C, with mean monthly temperature ranging from 8.8°C (July) to −27.2°C (January) (1998–2014). Summer rainfall averaged 56 mm from 2008 to 2014 (not corrected for undercatch).

Table 1
Overview of Meteorological and Hydrological Data Base (T, Air Temperature, RH, Air Humidity, WS, Wind Speed, SR, Solar Radiation, R, Rain, SN, Snow Depth, USGS, U.S. Geological Survey GTN-P Active-Layer Monitoring Site, Alaska)

Name/ID	Location (lat, lon, elevation)	Variables	Record length	Data source/agency
Meteorology				
Crea	70.3°N, −151.3°W, 5 m	T, RH, SR, WS, R	7/2011-present	Fish Creek watershed observatory[a]
Fish Creek	70.4°N, −152.1°W, 31 m	T, SR, WS, R, SN	8/1998–2014	USGS[b]
Inigok	70.1°N, −153.3°W, 53 m	T, SR, WS, R, SN	8/1998–2014	USGS[b]
Nuiqsut	70.2°N, −151.0°W, 17 m	T, RH, WS	2006–2014	Global surface hourly database[c]
Hydrology				
Crea	70.3°N, −151.3°W, 5 m	Runoff	2011–2019	Fish Creek watershed observatory[a]
Tundra Lake L9819, Lake L9820	70.3°N, −151.3°W, 5 m	End-of-winter snow accumulation	2010, 2011, 2012	Fish Creek watershed observatory[a]
Crea	70.3°N, −151.3°W, 5 m	Soil temperature (depths: ~1–2, 50, 100, 135 cm)	5/2013–2019	Fish Creek watershed observatory[a]

Note. All time series, except the end-of-winter snow accumulation, are available in hourly resolution.
[a]http://www.fishcreekwatershed.org/data.html. [b]http://pubs.usgs.gov/ds/812/introduction.html. [c]https://www7.ncdc.noaa.gov/CDO/cdopoemain.cmd?datasetabbv=DS3505%26countryabbv=%26georegionabbv=%26resolution=40.

We explicitly consider the two largest lakes within Crea Creek watershed: Upper and Lower Crea Lakes (Figure 1). Upper Crea Lake is a bedfast lake, that is, it freezes to the bottom in the winter, with a maximum measured lake depth of 1.1 m. Lower Crea Lake is deeper, with the maximum measured lake depth reaching 2.4 m and rarely freezes solid (Engram et al., 2018). Upper Crea Lake, has in most summers, ephemeral connectivity to Crea Creek while Lower Crea Lake's connectivity to Crea Creek is perennial (Heim et al., 2019). Lower Crea Lake is known to support several fish species during summer and potentially provides overwintering habitat based on dissolved oxygen data (Leppi et al., 2016).

Upper and Lower Crea lakes have historically supplied water and ice chips for petroleum exploration and development in the Lower Fish Creek watershed as part of the Greater Moose's Tooth 1 development project in the NPR-A (Arp et al., 2019). In 2017, a permanent gravel road was constructed that bisects the Crea Creek watershed with a bridge that crosses Crea Creek downstream of Lower Crea Lake. The assessments of pre- and post-development conditions have resulted in publications and reports describing fish distribution and movement (Heim et al., 2014, 2016; Morris, 2003), food web dynamics (McFarland et al., 2017), and hydrological and permafrost processes (Arp, Whitman, et al., 2015; Jorgenson & Shur, 2007). Currently, Upper and Lower Crea lakes supply water in both summer and winter for operations on the gravel road and nearby drilling pad. Due to the proximity of these lakes to the gravel road, they will likely be utilized for further water supply during the production phase.

3. Methods

3.1. Field Measurements for Model Forcing and Evaluation

The primary data and field measurements utilized in this study consisted of meteorological, hydrological (streamflow, snow accumulation, and end-of-winter snow water equivalent [SWE]) and soil temperature time series (Table 1). Spatial data sets include a digital elevation model (airborne LiDAR derived DEM of 0.25 m resolution, acquired 2013; Text S1 in Supporting Information S1; LiDAR, 2013), land cover (Payne et al., 2013), permafrost and surficial geology distribution (Jorgenson et al., 2014), which are used to parameterize the model.

Model forcing during model calibration and validation included hourly records of air temperature, precipitation, relative humidity, solar radiation, and wind speed at four meteorological stations located within or nearby Crea Creek watershed (Figure 1a, Table 1). Precipitation time series consists of rainfall measurements from three stations (Crea Creek, Fish Creek, Inigok) and estimated hourly water equivalent of snowfall from a sonic sensor of two stations (Fish Creek, Inigok). Precipitation was defined as 100% rainfall when air temperatures were $>-1°C$ and as 100% snowfall when air temperatures were $<-1°C$. Rainfall was measured at Crea Creek station, located in the lower portion of the Crea Creek watershed (Figure 1), using a non-shielded tipping bucket rain gauge (Onset RG3, 0.2 mm resolution). We corrected the rainfall measurements at Crea Creek station for undercatch using a factor of 1.8 based on field measurement presented in Yang et al. (1998). Fish Creek and Inigok stations are equipped with a shielded (ETI Instrument Systems Lexan altershield) rain gage (Texas Electronics TE 525).

Hourly snowfall water equivalent records to force the hydrological model were derived from snow depth recordings by sonic sensors (SR50-L, sensor height 2.5 m, Campbell Scientific, Logan, UT) following the method by Ryan et al. (2008). The hourly records of the sonic sensor were smoothed by a 24 hr moving average before summing up all positive changes to estimate snowfall amounts (Equation 1) and its water equivalent (Equation 2). The smoothing is necessary as estimates of snow depth are artificially variable during snowfall events caused by earlier returns of the signal from falling snow flakes that have not yet landed on the snowpack (Figure S1).

$$SF_D = \sum_{t=1}^{n} (SD_t - SD_{t-1}) \quad \text{for all } (SD_t > SD_{t-1}) \tag{1}$$

where SF_D is the depth of snowfall [m], SD is snow depths [m], t represents the time step (hourly) and n is the total number of time steps considered.

The water equivalent of the snowfall (SF_{SWE}) was estimated by multiplying the estimated hourly snowfall, (SF_D, Equation 1) by a temperature dependent snow density based on Hedstrom and Pomeroy (1998) and Judson and Doesken (2000) (Equation 2).

$$\text{SF}_{\text{SWE}} = \text{SF}_D * \frac{\rho}{\rho_w} \quad \begin{cases} \frac{\rho}{\rho_w} = 120\frac{\text{kg}}{\text{m}^3} \text{ if } T_a > -2°C \\ \frac{\rho}{\rho_w} = 100\frac{\text{kg}}{\text{m}^3} \text{ if } -2°C > T_a > -10°C \\ \frac{\rho}{\rho_w} = 80\frac{\text{kg}}{\text{m}^3} \text{ if } T_a < -10°C \end{cases} \qquad (2)$$

where ρ is snow density [kg m^{-3}], ρ_w is the density of water [kg m^{-3}], T_a is air temperature [°C], SF$_{\text{SWE}}$ is water equivalent of the freshly fallen snow [mm].

We also measured end-of-winter snow depth between 2011 and 2014 using a MagnaProbe (Sturm & Holmgren, 2018) on Lower Crea Lake and on the upland tundra. At each survey location, we applied the double sampling method with 50 depth measurements at 1 m intervals along northing and easting transects with five independent snow density samples collected per survey (Rovansek et al., 1993). In 2014, ~415 additional snow depths surveys were made with corresponding density sampling for each survey (locations shown in Figure 1c). Spiral snow depth transects covered a range of terrestrial and aquatic surfaces including beaded stream channels, lakes, DTLBs, and upland tundra to understand finer-scale snow storage variability within Crea Creek watershed. Active layer and shallow permafrost temperatures were recorded at the Crea Creek station (Table 1).

Crea Creek stream discharge has been gauged close to its confluence with the Ublutuoch River (Figure 1) beginning in 2009 as described in Arp, Whitman, et al. (2015) and Whitman et al. (2011). Discharge records were estimated from rating curves developed for a full range of flows from snowmelt peaks typically in early June to mid-summer low flows (>25 observations ranging from <0.001 to 1.5 m^3 s^{-1}) that were then applied to hourly creek water level observations using in situ pressure transducers. Discharge during ice-affected conditions when snow and ice in the channel impacted the relationship between stage and discharge (Pelletier, 1988; Shiklomanov et al., 2006), typically during the rising limb of the snowmelt hydrograph and during early winter (October and November), were estimated using exponential functions fit to field point discharge measurements (snowmelt rising limb) and aided by water temperature sensors and time-lapse cameras. Detailed information about the water level and discharge measurements are provided in the Supporting Information (Text S2 in Supporting Information S1).

3.2. The Hydrological Model WaSiM

The physically based, spatially fully distributed (regular grid cells) Water Balance Simulation Model (WaSiM, version 9.10.02.c; Schulla, 2019a), simulates water flux and storage as well as soil temperatures and heat transfer at the watershed scale. WaSiM is a permafrost hydrology watershed model with complexity similar to the Arctic Hydrology Model (Krogh et al., 2017), ARHYTHM (Z. Zhang et al., 2000), GEOtop 2.0 (Endrizzi et al., 2014), the hydrograph model (Vinogradov et al., 2011), and the Thermal Hydrology in the Arctic Terrestrial Simulator software (Jan et al., 2018; Painter et al., 2016).

The main capabilities that make WaSiM suitable for the application to watersheds located in tundra environment are:

- Fully distributed model, modular model structure, widely applied (>50 publications), physical basis of most model components
- The temperature and heat transfer module is fully integrated into the 1D soil water module (Richards equation), solving the Fourier law for heat conduction (Text S3 in Supporting Information S1, Supporting Information of Liljedahl et al., 2016). WaSiM simulates physically based ground temperature, thaw depth, and water movement within a seasonally freezing and thawing active layer as well as permafrost temperatures. The soil temperature module dynamically solves active layer depths and therefore allows for multi-year storage and movement of water (freezing/thawing of ground substrates including water, transport).
- Surface water routing including lake water fluctuations using 2D flow equation (Text S4 in Supporting Information S1)
- Snowmelt using an Energy Balance approach (calculates melt as well as sublimation)
- Optimized for parallel computing which makes its application efficient on computer clusters

WaSiM calculates snow accumulation and melt, evapotranspiration (including interception, sublimation, and moss/soil evaporation), and surface/subsurface water storage and movement. Table S1 details the chosen modules and algorithms for Crea Creek watershed. Simulations for this study were carried out with a spatial resolution of 10 m. The simulations time step is hourly, but for some modules (e.g., surface routing module) the simulation time step is reduced down to minutes or seconds to satisfy the Courant condition.

The topographic analysis tool (TANALYS; Schulla, 2019b) produced all the necessary topographic-derived geospatial data. Climate station data, including air temperature, precipitation, air humidity, radiation and wind speed, are interpolated onto the watershed scale using the inverse distance weighting approach. To represent snow distribution by wind, we developed a correction factor grid that accounts for differences in snow accumulation based on surface topographical features such as gullies (Figure S2, Text S5 in Supporting Information S1).

Four land cover and two soil types characterize the watershed (Figure S3). Parameterization of the land cover and unsaturated/saturated zone is shown in Tables S2 and S3, respectively. Land cover classes included wet sedges (41%), tussock tundra (40%), water/lakes bodies (10%), and shrubs (5%). The water/lakes cover class was additionally subdivided into shallow and deep-water bodies based on the lake classification detailed in Jones et al. (2017). To estimate ground surface temperatures for the soil temperature and heat transfer module (Text S3 in Supporting Information S1), *n*-factors were defined in a monthly resolution for each land cover type based on values reported in the literature (Kade et al., 2006; Lunardini, 1978; Table S2). *N*-factors present the ratio of ground-surface temperature to air temperature; thereby integrating the effects of all ground surface influences of the soil thermal regime. We used different *n*-factors for the shallow and deeper water bodies to account for the development of taliks under deeper water bodies. In addition, evaporation resistance was also set differently for shallow and deeper water to account for differences in the timing of lake ice-out (Arp, Jones, et al., 2015).

We simulated a vertical soil column of 28 m, discretizing layers of 10 cm thickness down to 2 m depth. The organic layer is 10 cm deep except in vegetated drained lake basins where we set a depth of 30 cm. We limited soil evaporation to the upper 10 cm of the soil column. Between 2 and 28 m soil depths, each soil layer has a thickness of 2 m. Soil properties were obtained from the literature (Daanen et al., 2007; Hinzman et al., 1991; O'Donnell et al., 2009; Price et al., 2008; Quinton et al., 2008; Y. Zhang et al., 2010).

We initialized the model with all the individual modules active by a 96 yr spin-up run to set permafrost temperatures at greater depths and realistic water storages in lakes as well as in the saturated and unsaturated zone. Hourly meteorological measurements from the year 2011, which represented average air temperature and precipitation, were used as spin-up forcing. The spin-up starts with a linear initialization of the soil temperature profile between the upper (air temperature set to measured mean annual air temperature of $-11°C$) and lower temperature boundary condition (defined as $-8°C$ at 28 m depth) obtained from the measured permafrost temperatures (Clow, 2014). After model initialization, we set a ground heat flux of 60 mW $(m^2)^{-1}$ as the lower boundary condition (Batir et al., 2013).

3.3. Model Calibration and Validation

The modeling strategy consists of a five-step approach (Figure 2). We ran the parallelized WaSiM code on 180 nodes awarded from the Extreme Science and Engineering Discovery Environment (XSEDE; Towns et al., 2014). During model set-up (steps 1 and 2), we pre-processed the model input data (meteorological records and spatial data sets) and parameterized the model. The multivariable calibration and validation were based on field measurements for the water years (1 October to 30 September) 2009–2011 and 2012–2014, respectively. During the first calibration loop, the parameters of the energy balance approach were adjusted to match observed and simulated end-of-winter SWE as well as timing and rate of snowmelt (Table S4). We compared simulated SWE to our measured end-of-winter SWE and average watershed-scale simulated to measured (from sonic sensor) snow ablation. Following the first calibration loop by fixing the calibrated snow-related parameters, we adjusted the surface roughness coefficient to best match simulated and measured discharge. The surface roughness is a measure of the amount of frictional resistance water experiences when passing over the land surface. We evaluated the WaSiM's performance against field measurements of snow depths/water equivalent, runoff, and soil temperature. Multiple statistical performance criteria (Coefficient of Determination (r^2), Index of Agreement (IoA; Willmott, 1981), root mean square error and Nash-Sutcliffe efficiency (NSE; Nash & Sutcliffe, 1970)) in combination with total
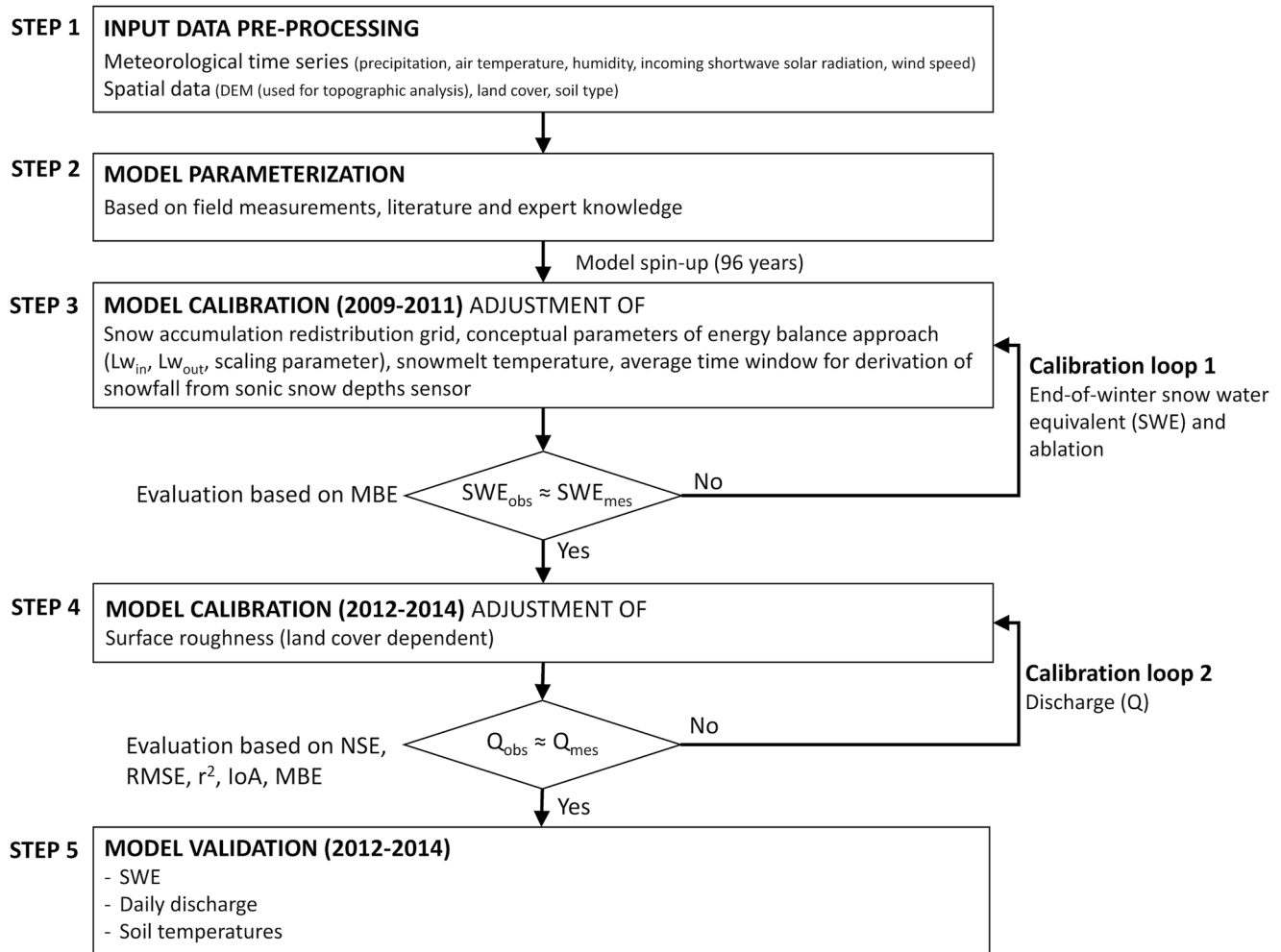
Figure 2. Modeling strategy for Crea Creek watershed. The modeling strategy includes a five-step approach including two calibration loops/iterations. Step 1 presents the input data preparation, step 2 the model parameterization, steps 3 and 4 the multi-step, multi-criteria model calibration, and step 5 the model validation. Step 3 is evaluated based on measured and simulated end-of-winter snow water equivalent (SWE), step 4 on measured and simulated discharge. Model performance is evaluated using different statistical indices: Mean Bias Error (MBE), Coefficient of Determination (r2), Nash Sutcliffe Efficiency (NSE), and Index of Agreement (IoA).

mass balance (MBE) were used to evaluate model accuracy by comparing daily simulated to measured discharge. The main calibrated model parameters are presented in Table S4.

3.4. Set-Up of Climate and Lake Water Withdrawal Scenarios

We developed four extreme climate scenarios, two LWW scenarios, and combinations thereof. In total 29 scenarios (Table S5) were set-up and compared to a control scenario. The climate forcing for the scenarios is based on the bias-adjusted simulated meteorological output of the Polar version of the Weather Research and Forecasting Model (WRF), which was forced by the observation-based ERA-interim reanalysis data (ERA-WRF) as detailed in Cai et al. (2018). Climate simulations output is available on a 10 km grid and at a three-hour temporal interval covering the period 1980–2014.

From the downscaled ERA-WRF record, we defined seasons (summer: June–September, winter: October–May) primarily based on their precipitation conditions. Our aim was to understand the hydrologic response caused by already observed extreme precipitation seasons. The following water year's and summer/winter periods were chosen from the downscaled ERA-WRF record (Table 2):

- Control: the water year closest to the average annual long-term precipitation and seasonal distribution. The control was obtained from year 1996 ($P_{JJAS} = 110$ mm, $P_{October–May} = 106$ mm).

Table 2
Overview of Meteorological Characteristics of the Years Chosen to Construct the Seasonal Climate Scenarios

	Year(s)	MAT [°C]	*P* [mm]
June–September			
C (and LWW)	1996	4.4	110
LR	2007	4.8	19
HR	2006	5.1	129
Average	1981–2014	4.6	100
October–May			
C (and LWW)	1996	−16.7	106
LS	1987	−19.2	64
HS	2014	−13.7	144
Average	1981–2014	−17.7	101

Notes. Mean air temperature (MAT) and precipitation (*P*) for the summer months (June–September) and winter months (October–May) are derived from bias-adjusted WRF output forced by reanalysis data (Cai et al., 2018). The values represent the average of six WRF grid cells covering the Crea Creek watershed. The scenario includes the control (C), lake water withdrawal (LWW), low rainfall (LR), high rainfall (HR), low snowfall (LS), and high snowfall (HS).

- LR (Figure 3): The summer (June–September) months with the lowest rainfall compared to the control. LR was obtained from the year of 2007 (P_{JJAS} = 19 mm, 17% of control). LR was complemented by control winter (October–May).
- Low snowfall (LS; Figure 3): The winter (October–May) months with the lowest snowfall compared to the control. LS was obtained from year 1987 ($P_{October–May}$ = 64 mm, 60% of control). LS was complemented by control summer (June–September).
- High rainfall (HR; Figure S4): The summer month (June–September) with the highest early season (June–August) precipitation compared to the control. HR obtained from year 2006 (P_{JJA} = 117 mm, 144% of control). HR was complemented by control winter (October–May).
- High snowfall (HS; Figure S5): The winter (October–May) months with the highest snowfall and air temperature compared to the control. HS was obtained from year 2014 ($P_{October–May}$ = 144 mm, 136% of control). HS was complemented by control summer (June–September).

Extreme climate seasons were not combined (e.g., LR and LS). As the extreme seasons present real observations, which means differences in precipitation amounts of the seasons (e.g., LR, LS) are not scaled equally to the control. For example, there is 91 mm less rainfall in the LR and 42 mm less in the LS scenario when compared to the control (Table 2). In addition, the other meteorological variables (air temperature, wind speed, humidity, and solar radiation) differ between the scenarios as we kept the original records from the chosen scenario year in order to keep the internal physical consistency between the meteorological variables. In this way, the chosen years/season
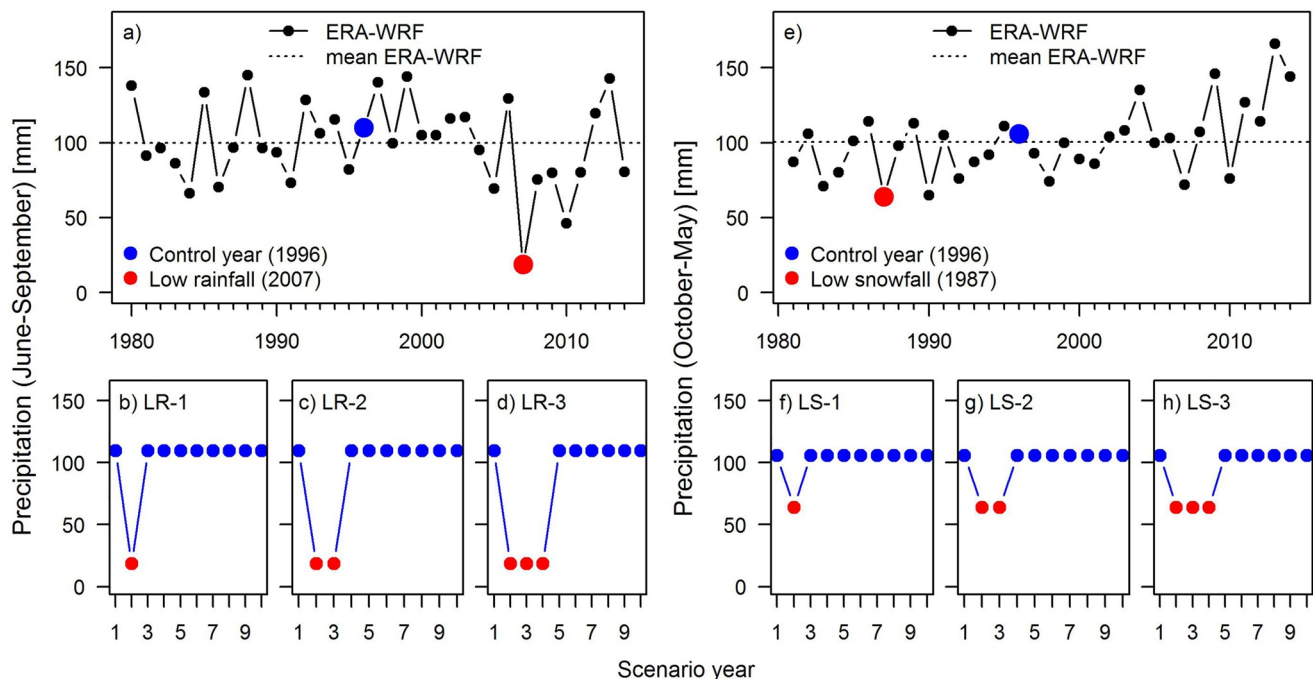
Figure 3. Example set-up of the extreme climate scenarios "Low Rainfall (LR)" and "Low Snowfall (LS)" based on the dynamically downscaled climate data (ERA-WRF). For the LR and LS scenarios, we selected an average (control) and the lowest rainfall summer (June–September, 17% of control) and lowest snowfall winter (October–May, 60% of control), respectively, from the ERA-WRF reanalysis rainfall time series (1980–2014) covering Crea Creek watershed (a, e). Based on the control and low rainfall year, we set up the scenarios LR-1 (b), LR-2 (c), and LR-3 (d). The LR scenario was accompanied by control winter forcing (October–May). The LS scenarios (LS-1 (f), LS-2 (g), LS-3 (h)) were accompanied by control summer forcing (June–September). Table S5 in the supporting details the set up.

Table 3
Indicators Used to Evaluate the Hydrologic Responses to the Climate and Lake Water Withdrawal Scenarios

Indicator [unit]	Description	Scenarios	Evaluation period
MQ7 [L s^{-1}]	Minimum 7-day mean flow (Richter et al., 1997)	All	Snowmelt peak - August
DCD [days]	Disconnectivity duration (flow threshold of 6.5 L s^{-1})	All	Consecutive days counted between snowmelt peak – August
Water balance [mm]	Water balance components (precipitation, evapotranspiration, runoff)	All	Average over May–August
Recovery time of MQ7 [days]	Recovery time of MQ7 to pre-perturbation conditions (=control ± 5%)	All	Snowmelt peak -August
Lake and DTLB outflow [m^3 s^{-1}]	The surface water flow at the drained thermokarst lake basin (DTLB) and Upper and Lower Crea Lake's outlets	Control, HR-3, LR-3, and LR-3 + LWW-S-3	June–August

Note. The scenarios are detailed in Table S5.

fully present meteorological conditions that have already been observed in the past. The chosen years/seasons were put together so that scenarios extended for 10 yr periods and were initialized by output of the 96 yr spin-up run. Year 1 had the control climate, year 2 (and 3, 4) had one extreme climate (LR, LS, HR, HS), and the remaining years had the control climate (Figure 3).

The LWW scenarios take the same approach, but instead water is extracted from the two major lakes in Crea Creek watershed (Upper and Lower Crea Lake, Figure 1) for a single year and stacked years (up to 9 yr). The LWW scenarios are forced by the control scenario climatology (Table 2). The withdrawal volumes were informed by maximum allowable, here referred to as "extreme" as the volume of lake ice is not considered, and typical amounts (removed in practice) under current regulations for lakes in the NPR-A (Arp et al., 2019). We set up single-lake extreme (LWW-S, Lower Crea Lake) and multiple lake typical (LWW-M, both Upper and Lower Crea Lake) water-use scenarios. For the LWW-S scenario, we reduced the lake water level of Lower Crea Lake (simulated lake volume after complete filling 1.1 hm^3) by manually reducing the surface water storage by 30% (315 mm) prior of snowmelt (30 January, restarting the model on 1 February). In the LWW-M scenarios, water is extracted at Upper and Lower Crea Lake during both winter (31 January) and summer (15 July). For the LWW-M, volumes are more representative of the actually permitted values. From Upper Crea Lake (simulated lake volume after complete filling 1.3 hm^3), 14% (145 mm) of total simulated lake volume is reduced during winter and 6% (62 mm) during summer while 7% (74 mm) and 2% (21 mm) are removed from Lower Crea Lake during winter and summer, respectively.

We also defined scenarios that combine LR and LWW-S to understand the combined hydrologic responses. For example, a 3 yr LR (years 2–4) with single-lake extreme water withdrawal for year 2 is scenario LR-3 + LWW-S-1.

3.5. Hydrological Indicators for Scenario Assessment

We evaluated hydrologic responses to the climate and LWW scenarios in terms of five indicators: water balance components (precipitation, evapotranspiration, runoff), minimum 7-day mean flow (MQ7), recovery time of MQ7 to control conditions, disconnectivity duration (DCD), and the surface water flow at the DTLB and Upper and Lower Crea Lake's outlets (Table 3). The DCD is based on a flow threshold of 6.5 L s^{-1}, which corresponds to stream water depths of ∼10 cm as estimated from measured hydraulic geometry at the gaging station at Crea Creek. Below this threshold, passage by large-bodied fish (e.g., adult Arctic grayling) is greatly limited (Baki et al., 2012; Heim et al., 2019). The threshold and hydraulic geometry relationship is specific to the Crea Creek channel near the gaging station, but we expect similar thresholds for fish passage in other beaded stream systems within the Fish Creek watershed (Jones et al., 2017). For all scenarios, the hydrological indicator is documented for the year following the last climate and/or LWW perturbation. For example, the impact of LR-1 on mean runoff is reported in simulation year 3 (year one: control, year two: LR).
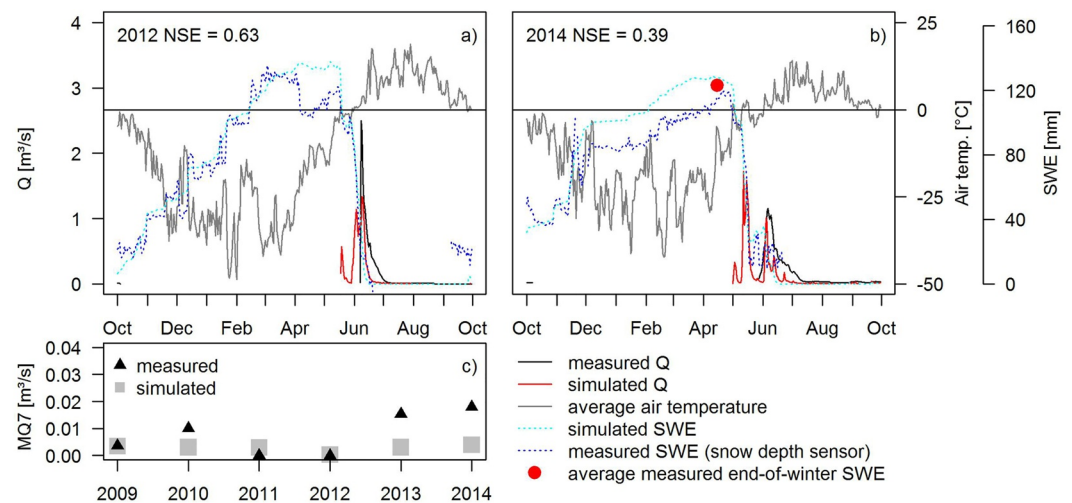
Figure 4. Measured and simulated daily discharge (Q), mean daily air temperature, daily snow water equivalent (SWE) and minimum 7-day mean flow (MQ7) for hydrologic years 2012 (a) and 2014 (b). Simulations were forced with meteorological measurements. Displayed are simulated (watershed average) and measured (at Fish Creek snow sensor) SWE (density 0.31 g cm^{-3}), average measured end-of-winter SWE, and watershed average air temperature (estimated from field stations using inverse distance weighting approach). Simulated discharge below 0.005 m^3 s^{-1} is not displayed. The calculated Nash Sutcliffe efficiency (NSE) between daily measured and simulated discharge is also indicated. Additional years (2009–2011, 2013) are presented in the Supporting Information (Figure S12). Measured and simulated minimum 7-day mean flow (MQ7; 2009–2014) are also displayed (c).

4. Results

4.1. Field Measurements and Hydrological Model Evaluation

End-of-winter snow depth point measurements average 24 and 16 cm on Lower and Upper Crea Lakes, respectively, and 40 cm on upland tundra (2012–2014). End-of-winter snow depth measured via spiral transects in 2014 (∼85 measurements at each location Figure 1c) showed that snow accumulation amounts and fine scale spatial variability correlate: in beaded streams, the highest mean snow depth and variability (68 ± 16 cm, mean ± standard deviation) was measured, followed by high centered polygons (44 ± 9 cm), lakes (28 ± 9 cm), DTLB (26 ± 7 cm) and low centered polygons (25 ± 4 cm). Measured snow density ranged from 210 (year 2014) to 310 kg m^{-3} (year 2012).

Simulated daily watershed-averaged SWE was slightly larger (+9% and +11% during calibration and validation, respectively) than the estimated point SWE from the sonic snow depth sensor at Fish Creek station located on upland tundra (Figure 4). The dynamic of daily SWE was well reproduced by WaSiM during calibration ($r^2 = 0.93$) and validation ($r^2 = 0.94$). Simulated end-of-winter SWE followed the observed spatial pattern of deeper snow accumulation on the tundra compared to Crea Lake (Figures S6a and S6b). The simulations overestimate measured SWE both on the Lower Crea Lake (25%, 2011–2014) and upland tundra surfaces (22%, 2012–2014) with the difference primarily attributed to year 2013. If the year 2013 is excluded from the records, the overestimation of SWE by the simulations is reduced to 9.8% on Lower Crea Lake and to 7.7% on the upland tundra. The simulated median SWE for the beaded stream channel and upland tundra fall within the spread of the measured SWE spiral transects in 2014 (Figure S6c). The measured small-scale SWE variability is not reproduced neither in the channel (interquartile range (IQR) IQR$_{measured}$ = 71, IQR$_{simulated}$ = 3.5) nor on the tundra (IQR$_{measured}$ = 31, IQR$_{simulated}$ = 0.3) by the simulations.

Measured snow ablation (by sonic depth sensor) starts in mid-May to early June, coinciding with air temperatures turning positive. Snow ablation takes between 8 (2010) and 34 (2014) days. Simulated onset and duration of snow ablation agrees well with the measurements (onset ±3 days, duration ±9 days in comparison to measurements), except in 2010 when WaSiM produced a delayed onset of snowmelt by 10 days resulting in the largest discrepancy between measurements and observations. The rapid simulated rate of snowmelt in 2010 resulted, however, in matching measured and simulated snowmelt peak timing (June 9th).

Following snow ablation, snowmelt runoff starts between late May to mid June. Simulated snowmelt runoff starts on average 19 days too early. Measured annual runoff, as estimated from stage-discharge relationships, averages 56 mm (2009–2014) ranging from 35 mm (2011) to 81 mm (2013) (Table S6). On average ~81% of the annual runoff occurs during a 20-day period following snowmelt, ranging from 60% (2014) to 92% (2012). In comparison, simulated annual runoff averages 45 mm between 2009 and 2014, which presents ~80% of measured runoff. Total annual runoff is underestimated by the model during both calibration (−12%, year 2009–2011) and validation (−17%, year 2012–2014). Model performance regarding simulated daily runoff is relatively consistent interannually (NSE ≥ 0.6), except in 2011 (NSE = −0.86) and 2014 (NSE = 0.39) (Table S7). WaSiM simulations overestimate peak discharge by on average 19% during calibration (year 2009–2011), while underestimating it by on average 34% during validation (year 2012–2014).

Average measured minimum 7-day mean flow (MQ7) is 4.5 L s^{-1} during calibration and 9.3 L s^{-1} during validation, averging to 6.9 L s^{-1} during the period 2009–2014. Measured MQ7 occurs on average around August 12th, ranging between the end of July (22 July 2013) and the end of August (25 August 2012). Simulated MQ7 averages to 2.8 L s^{-1} (2009–2014) and is underestimated compared to measured MQ7 during both calibration (−30%, 3.2 L s^{-1}) and validation (−74%, 2.4 L s^{-1}, Figure 4). The timing of the simulated MQ7 is delayed by on average 12 days (24 August).

Simulated runoff is approximately 25% of total annual precipitation, while 68% of total annual precipitation is lost as evapotranspiration (Table S6). The remaining 7% present changes in storages (lakes, soil- and groundwater). Evapotranspiration exceeds total rainfall (June–August) by on average 53 mm. Average simulated runoff coefficient during June through September is 0.4.

Active layer thickness is less than 50 cm at Crea Creek station (Figure S7). Annual average measured soil temperature is −3.4°C at 2 cm depth and −5.7°C at 135 cm depth (April 2013 to August 2014). Annual average simulated soil temperatures deviate by −0.1°C from the measurements close to the ground surface and by +0.2°C at 135 cm depth. At 100 cm depth, measured and simulated soil temperatures remain below 0°C throughout the year. The annual freeze-thaw cycle is well reflected by the model, as indicated by a coefficient of determination of 0.65 close to the ground surface and 0.92 at depths 135 cm (Figure S7). Near the ground surface, simulated soil temperatures show larger fluctuations compared to the measurements, likely caused by estimating the ground surface temperature by the *n*-factor approach. Results in large artificial soil temperature fluctuations. The simulated freezing and thawing occurs earlier and not as rapid compared to the measurements.

4.2. Scenarios

In the control scenario (presenting average climate conditions over the period 1980–2014), May through September precipitation (P_{MJJA}) totals to 105 mm, evapotranspiration (ET_{MJJA}) to 103 mm, and runoff (R_{MJJA}) to 57 mm. Low flow (MQ7) is 5.5 L s^{-1}. Fish passage is inhibited (DCD) for 6 days, lasting from 28 July to 2 August (Table 4).

4.2.1. Climate Scenarios

In the single to multiple years of LR (LR-1, LR-2, LR-3) and LS (LS-1, LS-2, LS-3), ET_{MJJA} exceeds P_{MJJA}. This results in a reduction of runoff (R_{MJJA}) by 18% following 1 yr to 33% following three consecutive years of LR and by 14% following one to 3 yr of LS (Table 4) compared to the control (R_{MJJA} = 57 mm). Low flows, represented by MQ7, decrease by 56% (25%) following 1 yr of LR (LS) and by 69% (33%) following three consecutive years of LR-3 (LS-3) (Figure 5, Table 4) compared to the control (MQ7 = 5.5 L s^{-1}) (Figure 5b, Table 4). The recovery time of MQ7 to control conditions takes three (two) years following LR (LS) scenarios. The number of fish non-passable days increases from 6 days in the control to 13 days following single to multiple LS years and up to 60 days following LR (LR-2, LR-3) years. The LR scenarios limit fish connectivity almost the entire warm season (3 Julyto 31 August [end of analysis period for DCD]) (Table 4). In the multi-year LR (LR-3) scenario, lake surface water outflow to Crea Creek reduces (Figure S8) at Upper Crea Lake (up to −57%), at the DTLB (up to −43%), and particularly at Lower Crea Lake (up to −68%) compared to control conditions.

In the single to multiple years of HR and HS scenarios, ET_{MJJA} is lower than P_{MJJA}. This results in increases in runoff (R_{MJJA}) by up to 35% (14%) following 3 yr of HR (HS) when compared to the control. Low flow (MQ7) increases following the HR (27%–42%) and the HS (5%–13%) scenarios compared to the control (Figure S9,

Table 4
Mean Seasonal Runoff (During Thawed Season (May–August)), Minimum 7-Day Mean Flow (MQ7), Disconnectivity Duration (DCD) and Timing of the Simulated Extreme Scenarios

Scenario		Mean runoff [mm]	MQ7 [L s^{-1}]	DCD [days]	Timing [month/day]	Duration [years]
Control	C	57	5.5	6	7/28-8/2	-
Low rainfall (LR)	LR-1	47	2.4	33	7/4-8/5	3
	LR-2	39	1.9	60	7/3-8/31	3
	LR-3	38	1.7	60	7/3-8/31	3
High rainfall (HR)	HR-1	77	7.0	2	7/12-7/13	1
	HR-2	74	7.4	-	-	2
	HR-3	75	7.8	-	-	2
Low snowfall (LS)	LS-1	49	4.1	13	7/27-8/8	2
	LS-2	49	3.8	13	7/27-8/8	2
	LS-3	49	3.7	13	7/27-8/8	2
High snowfall (HS)	HS-1	65	5.8	10	7/29-8/8	2
	HS-2	65	6.1	7	7/29-8/5	3
	HS-3	65	6.2	3	7/31-8/2	3
Lake water withdrawal (LWW)	LWW-S-1	33.5	3.1	15	7/26-8/9	2
	LWW-S-2	32.8	2.6	15	7/26-8/9	3
	LWW-S-3	32.8	2.3	15	7/26-8/14	3
	LWW-S-10	32.8	2.3	20	7/26-8/14	-
	LWW-M-1	33.5	3.3	14	7/27-8/9	2
	LWW-M-2	32.8	2.5	20	7/26-8/14	3
	LWW-M-3	32.7	2.3	20	7/26-8/14	3
LR-1 + LWW 1,2,3,10	LR-1 + LWW-S-1	24	1.0	64	6/29-8/31	3
	LR-1 + LWW-S-2	28	2.1	20	7/26-8/14	3
	LR-1 + LWW-S-3	33	2.3	15	7/26-8/9	3
	LR-1 + LWW-S-10	33	2.3	20	7/26-8/14	-
LR-2 + LWW 1, 2, 3	LR-2 + LWW-S-1	24	1.0	64	6/29-8/31	4
	LR-2 + LWW-S-2	20	0.7	64	6/29-8/31	3
	LR-2 + LWW-S-3	28	1.8	20	7/26-8/14	3
LR-3 + LWW 1, 2, 3	LR-3 + LWW-S-1	24	1.0	64	6/29-8/31	5
	LR-3 + LWW-S-2	19	0.7	64	6/29-8/31	4
	LR-3 + LWW-S-3	19	0.5	64	6/29-8/31	4

Notes. All indicators are calculated for the months May–August. Values are reported for the years of (last) disturbance (scenario-1: year 2, scenario-2: year 3, scenario-3: year 4, scenario-10: year 10). The recovery time assumes that the MQ7 returns to the control value ± 5%. The lake water withdrawal (LWW) scenario is differentiated between single LWW from only Lower Crea Lake (LWW-S) and multiple LWW where water is removed from both Upper and Lower Crea Lake.

Table 4). Recovery of MQ7 to pre-disturbance conditions takes one (HR-1) to 2 yr (HR-2, HR-3) following HR scenarios and two (HS-1) to 3 yr (HS-2, HS-3) following HS scenarios. DCD reduces from 6 days in the control to 2 days in a HR summer (HR-1). For multiple years of HR summer (HR-2, HR-3), fish connectivity is met throughout the summer. One to 2 yr of HS (HS-1, HS-2) do not affect DCD, but after three consecutive years of HS winters (HS-3), DCD reduces from six (control) to 3 days. Outflow from the lakes increases in the HR scenarios: by up to +83% at Upper Crea Lake, +45% at the DTLB to Crea Creek, and +160% at Lower Crea Lake compared to the control (Figures S8 and S10).
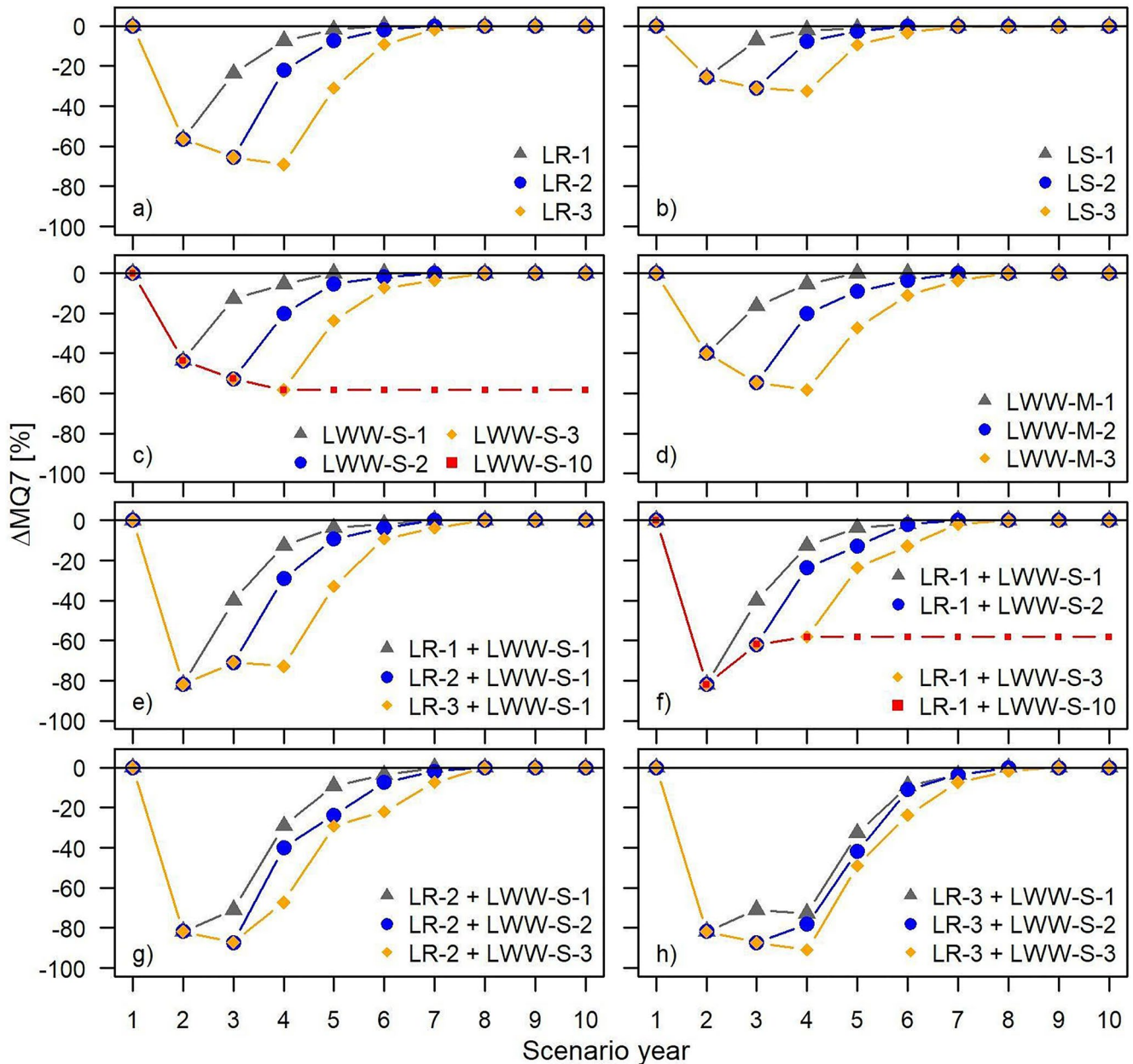
Figure 5. Impact of climate, lake water withdrawal, and combined scenarios on simulated minimum 7-day mean flow (MQ7). Displayed are the scenarios low rainfall (LR) (a), low snowfall (LS) (b), single-lake extreme water withdrawal (LWW-S) from Lower Crea Lake (c) and multi-lake typical LWW (LWW-M) from Upper and Lower Crea Lake (d) and combined low rainfall (LR) and LWW-S (c, h). The impact on the MQ7 is presented as percent differences to the control. The precipitation regime differs as follows between the scenarios: low rainfall summer ($P_{(JJAS)}$ 19 mm + $P_{(October–May)}$ 106 mm), low snowfall ($P_{(JJAS)}$ 110 mm + $P_{(October–May)}$ 64 mm), LWW ($P_{(JJAS)}$ 110 mm + $P_{(October–May)}$ 106 mm). The single and multi-year LWW scenarios are forced by the meteorological variables of the control scenario.

4.2.2. Lake Withdrawal and Combination of Lake Withdrawal and Low Summer Rainfall

Simulated runoff (R_{MJJA}) reduces by 41% (41%) following one and by 42.5% (42.6%) following 3 yr of single-lake extreme (multiple-lake typical) withdrawals compared to the control (Table 4). Lake water pumping is the sole cause for the reduction of R_{MJJA} because the climatic forcing is identical to the control scenario. Simulated MQ7 is reduced in the summer following water withdrawals (Table 4, Figures 5c and 5d). MQ7 decreases by a maximum of 58% after three to up to 10 yr of consecutive lake withdrawal (LWW-S-3, LWW-S-10, LWW-M-3), which is less compared to the LR (LR-3) scenario (69%, Figure 5a). Mean runoff (R_{MJJAS}) of the LWW scenarios, on the contrary, is lower compared to the LR scenarios (Figure S11 and Table 4) as the snowmelt event (when the

majority of runoff is generated) is comparable to control conditions in the LR scenarios. In addition, the total volume of lake water withdrawn in the LWW-S scenario is larger (315 mm) compared to the reduction of rainfall in LR (~64 mm [May–August]). The recovery time to control conditions takes 3 yr for all LWW scenarios, except for LWW-S-1/LWW-M-1 where it takes 2 yr (Table 4). Following 1–3 yr of LWW LWW-S (LWW-M), fish passage (DCD) is restricted for 15 (14) days. Under LWW-S (LWW-M), DCD increases to 20 days when lake water pumping occurs for more than 3 (1) consecutive years (Table 4). Lower Crea Lake disconnects from the drainage network after three consecutive winters of pumping (Figure 5c). A continued LWW in the following years (years 5–10) does not affect the MQ7 (Figure 5c) or the mean flow of Crea Creek (Table 4), but reduces lake water levels in Lower Crea Lake. The disconnection of Crea Creek from Lower Crea Lake suggests that the watershed (16.2 km^2) downstream of Lower Crea Lake contributes on average about 60% of the flow to MQ7 and 45% (180 mm) to the mean flow.

In the combined scenario of 1 yr of LR (LR-1) and 1 yr of single-LWW (LWW-S-1), runoff (R_{MJJAS}) decreases by 58% compared to the control and by 28% compared to the scenario LWW-S-1, where only LWW occurs with control climate. When 1–2 yr of only single LWWs (LWW-S) follow the combined LR-1 + LWW-S-1 scenario, R_{MJJAS} increases (following LS-1 + LWW-S-2 by 17%; following LS-1 + LWW-S-3/10 by 38%) but remains below the fish non-passable threshold (similar to the DCD values of the LWW scenarios). Following the combined scenario of 2 yr of consecutive LR summers and lake water pumping, runoff decreases by 65%. If an additional lake pumping year (with control climate) follows this scenario, runoff (R_{MJJA}) increases (from 20 to 28 mm) but is still only half compared to the control (57 mm). The largest reduction in R_{MJJAS} (−67%) occurs following the LR-3 combined with LWW-S-3 scenario, which has identical climate forcing compared to the LR-3 scenario, were R_{MJJAS} decreases by only 14%. Following the combined LR-3 and LWW-S-3 scenario, R_{MJJAS} almost ceases out of Crea Creek watershed (3.4 mm total runoff out of Crea Creek between June and August).

Low flow (MQ7) at Crea Creek outlet reduces considerably under the combined impact of LR and single-LWW (LWW-S) compared to the control (Table 4). After 1 yr of LR combined with LWW-S (LR-1 + LWW-S-1), MQ7 reduces by 82%. When additional years of lake water pumping follow a year of combined LR and lake water pumping, MQ7 is comparable to following two to 3 yr of solely single lake water pumping (LWW-S-2/3, Figures 5f and 5g, Table 4). When LR summers continue to occur after a combined scenario of LR and lake water pumping, MQ7 is less compared to following only LR summers. MQ7 even continues to decrease as the example of the combination LR-3 + LWW-S-1 in Figure 5h shows. Overall, MQ7 is higher for the LR-1 + LWW-S-3 (−58% to control) compared to the LR-3 + LWW-S-1 (−82% to control) scenario, which shows that low flows are more strongly affected by LR compared to LWW. MQ7 is most affected following 3 yr of combined LR and LWW (LR-3 + LWW-S-3) when a reduction by 91% (MQ7 = 0.5 L s^{-1}) is simulated and the recovery to control conditions takes 4 yr.

As a result of more severe low flows under the combined LR + LWW-S scenarios, fish passage (DCD) is limited for a majority of the warm season (64 days, 29 June to 31 August). When LWW-S follows the combined impact of LR and LWW-S, DCD decreases to 20 days (26 July to 14 August, LR -1 + LWW-S-2) and 15 days (26 July to 9 August, LR-1 + LWW-S-3). A DCD of 15 days corresponds to those of the LWW-S scenarios following two to 3 yr of LWW. Surface lake water outflow of Lower Crea Lake ceases entirely when LR occurs in the same year as LWW-S (Figures S8b and S11). Lower Crea Lake begins to feed the stream again after 3 yr of recovery time. Surface water outflow from Upper Crea Lake and the DTLB outlet to Crea Creek nearly cease entirely (only 1% of flow compared to control) in the third year of cumulative LR and LWW-S.

5. Discussion

5.1. Challenges of Modeling Hydrological Processes in Low-Gradient Arctic Tundra Watersheds

The multi-objective and multi-criteria model validation showed that WaSiM mostly simulates hydrological and thermal fluxes reliably in the low-gradient tundra environment of Crea Creek watershed, ACP, Alaska. Model performance is comparable to other studies, such as Krogh et al. (2017), Liljedahl et al. (2016), and Z. Zhang et al. (2000). The differences in modeled and field-estimated timing and amount of snowmelt runoff are likely a combined effect of uncertainty in and lack of field observations (e.g., measured snowfall, end-of-winter watershed snow distribution, estimating discharge during snow- and ice-affected conditions) as well as model limitations. Our approach to estimate snowfall time series from sonic snow depth sensors and our manually created

spatial snow accumulation distribution grid is a simplified representation of snow distribution by strong winds, which are characteristic of low-gradient Arctic tundra environments (Fischer, 2011; Ryan et al., 2008), and the smaller-scale heterogeneity of snow distribution across the landscape (Woo, 1986). Recent developments of blowing snow transport and sublimation models show promising results (e.g., Pomeroy & Li, 2000) and their integration into catchments models has the potential to refine water balance estimates in tundra environments. For example, Marsh et al. (2020) presented a three-dimensional blowing snow model based on a variable resolution unstructured mesh that considerably improved SWE estimates in a subarctic mountain basin. In our tundra environment, we used a simpler approach, which allowed us to reproduce the dominant snow spatial distribution patterns. Nevertheless, we acknowledge that efficient blowing snow transport models would improve water balance modeling studies on the watershed scale.

WaSiM realistically represented the snowmelt rates and the timing of the snow-free dates, while the onset and peak flow of simulated snowmelt runoff is too early in most years from field-based estimations at the watershed outlet. Similar results were obtained using the ARHYTHM model when applied to a tundra watershed in northern Alaska (Z. Zhang et al., 2000). The uncertainty is largest during the rising limb of snowmelt hydrograph when the channel is ice affected and the early snowmelt water is stored in the snowpack. During this period, stage-discharge relationships are not applied, and flow records are interpolated between point measurements or extrapolated to the rated peak. Damming of meltwater within the stream channel or upstream drained lake basins can cause rapid flow peaks during the rise limb period (Arp, Jones, et al., 2020). These processes are not simulated in this model, and often missed by standard stream gaging. Further, in tundra environments, meltwater often re-freezes within or at the bottom of the snowpack (Kane et al., 1991; Woo, 1986) and lateral snow-damming of meltwater is common (Brown et al., 1968; Woo & Guan, 2006). Both of these processes can have a delaying effect of several days on the streamflow response to snowmelt. The model version applied here represents snow cover as a single layer with a pre-defined meltwater storage capacity that does not allow for re-freezing of meltwater. The model is also not representing snow-damming effects of meltwater as the processes of snowmelt and surface water routing are decoupled modules. Considering the model design, it is reasonable that the model produced, on average, too early runoff response to snowmelt. Another important aspect is that our model version of WaSiM does not simulate freeze/thaw of surface water in stream channels. Consequently, ice jams, which are very common in such environments (Woo, 1986), and their delaying effect on watershed runoff, are not considered. Although we set model parameters (Tables S2 and S3) based on field observations and values reported in the literature we acknowledge the uncertainty induced by them. Lastly, the model resolution (10 m) does not resolve ice-wedge polygon features such as troughs (some form early stream networks) that are characteristic for Arctic tundra environments. Ice-wedge polygon microtopography considerably affects the spatial distribution of snow on the landscape, the timing and shape of the snowmelt hydrograph, and the overall partitioning of runoff and surface water storage (Liljedahl et al., 2016).

5.2. Seasonal Climate Extremes and Lake Water-Withdrawal Scenarios

Our scenario simulations showed that seasonal climate extremes and lake water-withdrawal have an immediate impact on streamflow and lake water levels, and therefore directly affect fish stream habitat connectivity. The stacked multi-year scenarios show a nonlinear response to the combined or individual climate and LWW perturbations. The scenario impact is strongest in the first year after which the absolute impact reduces. In the case of the LWW scenarios, a new hydrological equilibrium is reached after three consecutive years (Table 4) where the watershed contributing area is considerably reduced.

LWW scenarios, where all (LWW-S) or the majority of (LWW-M) water is pumped in prior to snowmelt, affects the water balance of the watershed for at least 2 yr. Therefore, the effect of winter LWW is not offset by the following spring snowmelt recharge as currently assumed in land management regulations. Regional snowfall scenarios for the study area, for example, Cai et al. (2018), project increasing snowfall rates which may offset LWWs to a certain degree in the future.

Under the combined LR and lake pumping (LR-3 + LWW-S-3) scenario, we find that surface flows out of Lower Crea Lake become disconnected between June and August over a 5 yr period (Figure S8b). Simulated outflows of Upper Crea Lake and the DTLB also almost entirely cease (Figures S8a and 8c). As a consequence, streamflow of Crea Creek falls below the fish passable threshold for the majority of the summer season in the most extreme scenario (LR-3 + LWW-S-3). The fragmentation of the surface water network and the resulting low flows in

the Crea Creek limit fish migration into the lakes in early summer for foraging and prevent a return of the fish to downstream overwintering habitat in late summer (Heim et al., 2016). Such changes will, if occurring with increased frequency, likely modify fish species distribution and fish assemblage composition of these habitats (Laske et al., 2016).

Lower lake water levels affect not only the water balance but also the lake ice-regime. Reduced lake water levels at the end of summer combined with low air temperatures can increase the likelihood of lake ice freezing to the bottom (bedfast ice lake) during winter (Arp, Jones, et al., 2012). Bedfast ice lakes do not provide access to water in winter for industry nor aquatic habitat (Arp, Jones, et al., 2015). However, warmer winter air temperatures and increased lake ice snow accumulation may instead thin lake ice to allow floating ice and, therefore, potentially offset low lake water levels that are caused by LR and winter LWW. Lake ice regimes (bedfast vs. floating) do not only affect freshwater habitat and water supply, but also lake ice-out timing, evaporation, and lake thermal regime (Arp, Jones, et al., 2015), which are additional examples of cascading impacts of LWW on the tundra lake hydrology.

The winter perturbations primarily affect snowmelt runoff (+18% (HS), −29% (LS)) the main hydrological event in the study area. Therefore, winter perturbations impact is less on late summer low flows. Excess water during snowmelt fills up surface storages (lakes, DTLBs, and other surface depressions) that recharge the active layer during summer and sustain late summer flows. Our simulations also show that mean runoff after two (HR-2) and three (HR-3) consecutive years of HR is lower compared to only 1 yr (HR-1). This is most likely caused by larger scale watershed inundation for HR-2 and HR-3 where water spills over lake/creek boundaries and is stored and/ or evaporatranspirated from the landscape instead of leaving the watershed as runoff.

Based on our study results, the following considerations may be helpful to regional land managers:

- Lakes water volumes pumped and the long-term amounts naturally recharged should be in balance. Ensuring that water pumped from individual lakes remains within its watershed to help offset this deficit through potential return-flow may aid in attaining this goal (understanding however that much of this extracted water will likely be lost to evapotranspiration).
- Lake-centric geospatial databases (i.e., Jones et al., 2017), catchment-specific geospatial databases (i.e., Johaneman et al., 2020), and satellite images (White et al., 2008) can provide site specific information on lake and stream connectivity and lake ice-regime to prevent bedfast lake ice and stream disconnectivity.
- Prioritizing isolated lakes (and lakes located not within the main contributing area of the watershed) for LWW instead of lakes with perennial connection to the stream networks that serve as migrating corridors for fish would mitigate negative effects to local biota. In addition, isolated bed-fast ice lakes may serve as viable low-impact source of early winter water and ice chip extraction as they do not provide important overwintering habitat for fish (Arp, Jones, et al., 2015).
- The storage capacity of the lakes relative to outlet elevations, which determines a lakes storage excess and deficit, may be considered in managing maximum allowable withdrawal amounts in order to help ensure downstream connectivity relative to meteoric water balance variability.
- Individual LWW may need to be restricted to every two or 3 yr to allow a system recovery (i.e., fully recharge) in between pumping.
- Flexible permits will allow quick reactions to climate extremes.
- Flexible water management: For example, in LR years (and those following), restricting lake water pumping permits may be helpful for avoiding excessive water withdrawals, while in years with HR, allowing generous water permits may be possible.
- Making informed management decisions under greater climatic variability requires sustained observations to establish an early warning system and qualified decision makers.

6. Conclusions

Through field and modeling efforts, we demonstrate that winter LWW (LWW) as applied by industry on the ACP, Alaska, is not reliably offset by same-year snowmelt recharge as currently assumed in land management regulations. A tundra lake is commonly pumped for multiple winters, particularly for newly developed areas with built infrastructure and year-round operations as is now the case for the Crea Creek watershed. Our simulations show that 3 yr of LWW results in a new hydrologic equilibrium in low flow and runoff that produce several weeks of

impassable stream conditions for fish during migration periods. Further, in the Crea Creek watershed, LWW in lakes located in the primary watershed contributing area has a larger effect on low flow than pumping of lakes that are not permanently connected to the stream network. Depending on summer rainfall amounts, the recovery time from multi-year LWW ranges from two to 5 yr as 1 yr of snowmelt is not sufficient to replenish surface water deficits. An increased climate variability with LR years combined with business as usual in regard to LWW regulations could potentially trigger irreversible system changes for aquatic habitats processes.

Data Availability Statement

All data sources are cited in the manuscript or in the Supporting Information. The WRF climate forcing data is available at Cai et al. (2018). The WaSiM model code (version 9.10.02.c) can be downloaded from: http://www.wasim.ch/en/products/release_r_old_versions.htm.

References

Arp, C. D., Jones, B. M., Hinkel, K. M., Kane, D. L., Whitman, M. S., & Kemnitz, R. (2020). Recurring outburst floods from drained lakes: An emerging Arctic hazard. *Frontiers in Ecology and the Environment*, *18*(7), 384–390. https://doi.org/10.1002/fee.2175

Arp, C. D., Jones, B. M., Liljedahl, A. K., Hinkel, K. M., & Welker, J. A. (2015). Depth, ice thickness, and ice-out timing cause divergent hydrologic responses among Arctic lakes. *Water Resources Research*, *51*(12), 9379–9401. https://doi.org/10.1002/2015WR017362

Arp, C. D., Jones, B. M., Lu, Z., & Whitman, M. S. (2012). Shifting balance of thermokarst lake ice regimes across the Arctic Coastal Plain of northern Alaska. *Geophysical Research Letters*, *39*(16), L16503. https://doi.org/10.1029/2012GL052518

Arp, C. D., Whitman, M. S., Jones, B. M., Grosse, G., Gaglioti, B. V., & Heim, K. C. (2015). Distribution and biophysical processes of beaded streams in Arctic permafrost landscapes. *Biogeosciences*, *12*(1), 29–47. https://doi.org/10.5194/bg-12-29-2015

Arp, C. D., Whitman, M. S., Jones, B. M., Kemnitz, R., Grosse, G., & Urban, F. E. (2012). Drainage network structure and hydrologic behavior of three lake-rich watersheds on the Arctic Coastal Plain, Alaska. *Arctic Antarctic and Alpine Research*, *44*(4), 385–398. https://doi.org/10.1657/1938-4246-44.4.385

Arp, C. D., Whitman, M. S., Jones, B. M., Nigro, D. A., Alexeev, V. A., Gädeke, A., et al. (2019). Ice roads through lake-rich Arctic watersheds: Integrating climate uncertainty and freshwater habitat responses into adaptive management. *Arctic Antarctic and Alpine Research*, *51*(1), 9–23. https://doi.org/10.1080/15230430.2018.1560839

Arp, C. D., Whitman, M. S., Kemnitz, R., & Stuefer, S. L. (2020). Evidence of hydrological intensification and regime change from northern Alaskan watershed runoff. *Geophysical Research Letters*, *47*(17), e2020GL089186. https://doi.org/10.1029/2020GL089186

Baki, A. B. M., Zhu, D. Z., Hulsman, M. F., Lunn, B. D., & Tonn, W. M. (2012). The hydrological characteristics of a stream within an integrated framework of lake-stream connectivity in the Lac de Gras Watershed, Northwest Territories, Canada. *Canadian Journal of Civil Engineering*, *39*(3), 279–292. https://doi.org/10.1139/l11-129

Batir, J. F., Blackwell, D. D., & Richards, M. C. (2013). Updated surface heat flow map of Alaska. *Geothermal Resources Council-Transactions*, *37*, 2–23.

Betts, E. D., & Kane, D. L. (2015). Linking North Slope of Alaska climate, hydrology, and fish migration. *Hydrology Research*, *46*(4), 578–590. https://doi.org/10.2166/nh.2014.031

Bowling, L. C., Kane, D. L., Gieck, R. E., Hinzman, L. D., & Lettenmaier, D. P. (2003). The role of surface storage in a low-gradient Arctic watershed. *Water Resources Research*, *39*(4), 1087. https://doi.org/10.1029/2002WR001466

Brown, J., Dingman, S. L., & Lewellen, R. I. (1968). *Hydrology of a drainage basin on the Alaskan Coastal Plain, DTIC document report*, (p. 24018). U.S. Army CRREL Research Report.

Cai, L., Alexeev, V. A., Arp, C. D., Jones, B. M., Liljedahl, A. K., & Gädeke, A. (2018). The polar WRF downscaled historical and projected twenty-first century climate for the coast and foothills of Arctic Alaska. *Frontiers of Earth Science*, *5*(111). https://doi.org/10.3389/feart.2017.00111

Clow, G. D. (2014). Temperature data acquired from the DOI/GTN-P deep borehole array on the Arctic slope of Alaska, 1973–2013. *Earth System Science Data*, *6*(1), 201–218. https://doi.org/10.5194/essd-6-201-2014

Daanen, R. P., Misra, D., & Epstein, H. E. (2007). Active-layer hydrology in nonsorted circle ecosystems of the Arctic tundra. *Vadose Zone Journal*, *6*, 694–704. https://doi.org/10.2136/vzj2006.0173

Déry, S. J., Stahl, K., Moore, R. D., Whitfield, P. H., Menounos, B., & Burford, J. E. (2009). Detection of runoff timing changes in pluvial, nival, and glacial rivers of western Canada. *Water Resources Research*, *45*(4). https://doi.org/10.1029/2008WR006975

Endrizzi, S., Gruber, S., Dall'Amico, M., & Rigon, R. (2014). GEOtop 2.0: Simulating the combined energy and water balance at and below the land surface accounting for soil freezing, snow cover, and terrain effects. *Geoscientific Model Development*, *7*(6), 2831–2857. https://doi.org/10.5194/gmd-7-2831-2014

Engram, M., Arp, C. D., Jones, B. M., Ajadi, O. A., & Meyer, F. J. (2018). Analyzing floating and bedfast lake ice regimes across Arctic Alaska using 25 yr of space-borne SAR imagery. *Remote Sensing of Environment*, *209*, 660–676. https://doi.org/10.1016/j.rse.2018.02.022

Fischer, A. M. (2011). The measurement factors in estimating snowfall derived from snow cover surfaces using acoustic snow depth sensors. *Journal of Applied Meteorology and Climatology*, *50*(3), 681–699. https://doi.org/10.1175/2010jamc2408.1

Hedstrom, N. R., & Pomeroy, J. W. (1998). Measurements and modeling of snow interception in the boreal forest. *Hydrological Processes*, *12*(10–11), 1611–1625. https://doi.org/10.1002/(SICI)1099-1085(199808/09)12:10/11<1611::AID-HYP684>3.0.CO;2-4

Heim, K. C., Arp, C. D., Whitman, M. S., & Wipfli, M. S. (2019). The complementary role of lentic and lotic habitats for Arctic grayling in a complex stream-lake network in Arctic Alaska. *Ecology of Freshwater Fish*, *28*(2), 209–221. https://doi.org/10.1111/eff.12444

Heim, K. C., Wipfli, M. S., Whitman, M. S., Arp, C. D., Adams, J., & Falke, J. A. (2016). Seasonal cues of Arctic grayling movement in a small Arctic stream: The importance of surface water connectivity. *Environmental Biology of Fishes*, *99*(1), 49–65. https://doi.org/10.1007/s10641-015-0453-x

Heim, K. C., Wipfli, M. S., Whitman, M. S., & Seitz, A. C. (2014). Body size and condition influence migration timing of juvenile Arctic grayling. *Ecology of Freshwater Fish*, *25*(1), 156–166. https://doi.org/10.1111/eff.12199

Hinzman, L. D., Kane, D. L., Gieck, R. E., & Everett, K. R. (1991). Hydrologic and thermal properties of the active layer in the Alaskan Arctic. *Cold Regions Science and Technology*, *19*(2), 95–110. https://doi.org/10.1016/0165-232X(91)90001-W

Jan, A., Coon, E. T., Painter, S. L., Garimella, R., & Moulton, J. D. (2018). An intermediate-scale model for thermal hydrology in low-relief permafrost-affected landscapes. *Computational Geosciences*, *22*(1), 163–177. https://doi.org/10.1007/s10596-017-9679-3

Johaneman, T. M., Arp, C. D., Whitman, M. S., Bondurant, A. C., Hamann, H. B., & Kerwin, M. W. (2020). Classifying connectivity to guide aquatic habitat management in an arctic coastal plain watershed experiencing land use and climate change. *Arctic Antarctic and Alpine Research*, *52*(1), 476–490. https://doi.org/10.1080/15230430.2020.1805848

Jones, B. M., Arp, C. D., Hinkel, K. M., Beck, R. A., Schmutz, J. A., & Winston, B. (2009). Arctic lake physical processes and regimes with implications for winter water availability and management in the National Petroleum Reserve Alaska. *Environmental Management*, *43*(6), 1071–1084. https://doi.org/10.1007/s00267-008-9241-0

Jones, B. M., Arp, C. D., Whitman, M. S., Nigro, D., Nitze, I., Beaver, J., et al. (2017). A lake-centric geospatial database to guide research and inform management decisions in an Arctic watershed in northern Alaska experiencing climate and land-use changes. *Ambio*, *46*, 769–786. https://doi.org/10.1007/s13280-017-0915-9

Jones, B. M., Grosse, G., Arp, C. D., Jones, M. C., Walter Anthony, K. M., & Romanovsky, V. E. (2011). Modern thermokarst lake dynamics in the continuous permafrost zone, northern Seward Peninsula, Alaska. *Journal of Geophysical Research: Biogeosciences*, *116*(G2), G00M03. https://doi.org/10.1029/2011JG001666

Jones, B. M., Grosse, G., Arp, C. D., Miller, E., Liu, L., Hayes, D. J., & Larsen, C. F. (2015). Recent Arctic tundra fire initiates widespread thermokarst development. *Scientific Reports*, *5*, 15865. https://doi.org/10.1038/srep15865

Jorgenson, M. T., Kanevskiy, M., Shur, Y., Grunblatt, J., Ping, C. L., & Michaelson, G. J. (2014). Permafrost database development, characterization, and mapping for northern Alaska. Retrieved from http://file-sctc.gina.alaska.edu/public/NoAKPermafrost_Mapping.pdf

Jorgenson, M. T., & Shur, Y. (2007). Evolution of lakes and basins in northern Alaska and discussion of the thaw lake cycle. *Journal of Geophysical Research: Earth Surface*, *112*(F2), F02S17. https://doi.org/10.1029/2006JF000531

Jorgenson, M. T., Shur, Y. L., & Pullman, E. R. (2006). Abrupt increase in permafrost degradation in Arctic Alaska. *Geophysical Research Letters*, *33*(2), L02503. https://doi.org/10.1029/2005GL024960

Judson, A., & Doesken, N. (2000). Density of freshly fallen snow in the central Rocky mountains. *Bulletin of the American Meteorological Society*, *81*(7), 1577–1588. https://doi.org/10.1175/1520-0477(2000)081<1577:Doffsi>2.3.Co;2

Kade, A., Romanovsky, V. E., & Walker, D. A. (2006). The *n*-factor of nonsorted circles along a climate gradient in Arctic Alaska. *Permafrost and Periglacial Processes*, *17*(4), 279–289. https://doi.org/10.1002/ppp.563

Kane, D. L., Hinzman, L. D., Benson, C. S., & Liston, G. E. (1991). Snow hydrology of a headwater Arctic basin: I. Physical measurements and process studies. *Water Resources Research*, *27*(6), 1099–1109. https://doi.org/10.1029/91wr00262

Krogh, S. A., Pomeroy, J. W., & Marsh, P. (2017). Diagnosis of the hydrology of a small Arctic basin at the tundra-taiga transition using a physically based hydrological model. *Journal of Hydrology*, *550*, 685–703. https://doi.org/10.1016/j.jhydrol.2017.05.042

Laske, S. M., Haynes, T. B., Rosenberger, A. E., Koch, J. C., Wipfli, M. S., Whitman, M. S., & Zimmerman, C. E. (2016). Surface water connectivity drives richness and composition of Arctic lake fish assemblages. *Freshwater Biology*, *61*, 1090–1104. https://doi.org/10.1111/fwb.12769

Leppi, J. C., Arp, C. D., & Whitman, M. S. (2016). Predicting late winter dissolved oxygen levels in Arctic lakes using morphology and landscape metrics. *Environmental Management*, *57*, 463–473. https://doi.org/10.1007/s00267-015-0622-x

Lesack, L. F. W., & Marsh, P. (2010). River-to-lake connectivities, water renewal, and aquatic habitat diversity in the Mackenzie River Delta. *Water Resources Research*, *46*(12). https://doi.org/10.1029/2010WR009607

LiDAR. (2013). *Epscor Northern Test Case*. Arctic Data Center. 43bc1629-233c-4944-af79-dfd2f0c00840.

Liljedahl, A. K., Boike, J., Daanen, R. P., Fedorov, A. N., Frost, G. V., Grosse, G., et al. (2016). Pan-Arctic ice-wedge degradation in warming permafrost and its influence on tundra hydrology. *Nature Geoscience*, *9*(4), 312–318. https://doi.org/10.1038/ngeo2674

Liljedahl, A. K., Hinzman, L. D., Harazono, Y., Zona, D., Tweedie, C. E., Hollister, R. D., et al. (2011). Nonlinear controls on evapotranspiration in arctic coastal wetlands. *Biogeosciences*, *8*(11), 3375–3389. https://doi.org/10.5194/bg-8-3375-2011

Liljedahl, A. K., Hinzman, L. D., Kane, D. L., Oechel, W. C., Tweedie, C. E., & Zona, D. (2017). Tundra water budget and implications of precipitation underestimation. *Water Resources Research*, *53*(8), 6472–6486. https://doi.org/10.1002/2016WR020001

Lunardini, V. J. (1978). *Theory of N-factors and correlation of data*, paper presented at Proceedings of the Third International Conference on Permafrost.National Counsel of Canada.

Marsh, C. B., Pomeroy, J. W., Spiteri, R. J., & Wheater, H. S. (2020). A finite volume blowing snow model for use with variable resolution meshes. *Water Resources Research*, *56*(2), e2019WR025307. https://doi.org/10.1029/2019WR025307

McFarland, J. J., Wipfli, M. S., & Whitman, M. S. (2017). Trophic pathways supporting Arctic grayling in a small stream on the Arctic Coastal Plain, Alaska. *Ecology of Freshwater Fish*, *27*, 184–197. https://doi.org/10.1111/eff.12336

Morris, W. (2003). *Seasonal movements and habitat use for Arctic grayling (Thymallus arcticus), burbot (Lota lota), and broad whitefish (Coregonus nasus) with the Fish Creek drainage of the National Petroleum Reserve - Alaska, 2001-2002*. Alaska Department of Natural Resources, Office of Habitat Management and Permitting.

Nash, J. E., & Sutcliffe, J. V. (1970). River flow forecasting through conceptual models part I—A discussion of principles. *Journal of Hydrology*, *10*(3), 282–290. https://doi.org/10.1016/0022-1694(70)90255-6

O'Donnell, J. A., Romanovsky, V. E., Harden, J. W., & McGuire, A. D. (2009). The effect of moisture content on the thermal conductivity of moss and organic soil horizons from black spruce ecosystems in interior Alaska. *Soil Science*, *174*(12), 646–651. https://doi.org/10.1097/SS.0b013e3181c4a7f8

Oelke, C., Zhang, T., & Serreze, M. C. (2004). Modeling evidence for recent warming of the Arctic soil thermal regime. *Geophysical Research Letters*, *31*(7), L07208. https://doi.org/10.1029/2003GL019300

Painter, S. L., Coon, E. T., Atchley, A. L., Berndt, M., Garimella, R., Moulton, J. D., et al. (2016). Integrated surface/subsurface permafrost thermal hydrology: Model formulation and proof-of-concept simulations. *Water Resources Research*, *52*(8), 6062–6077. https://doi.org/10.1002/2015WR018427

Payne, J., Guyer, S., Fehringer, D., & Boggs, K. (2013). North slope science initiative landcover mapping summary report. Retrieved from http://catalog.northslope.org/catalog/entries/8309

Pelletier, P. M. (1988). Uncertainties in the single determination of river discharge: A literature review. *Canadian Journal of Civil Engineering*, *15*(5), 834–850. https://doi.org/10.1139/l88-109

Pomeroy, J. W., & Li, L. (2000). Prairie and arctic areal snow cover mass balance using a blowing snow model. *Journal of Geophysical Research: Atmospheres*, *105*(D21), 26619–26634. https://doi.org/10.1029/2000JD900149

Price, J. S., Whittington, P. N., Elrick, D. E., Strack, M., Brunet, N., & Faux, E. (2008). A method to determine unsaturated hydraulic conductivity in living and undecomposed Sphagnum moss. *Soil Science Society of America Journal*, *72*(2), 487–491. https://doi.org/10.2136/sssaj2007.0111N

Quinton, W. L., Hayashi, M., & Carey, S. K. (2008). Peat hydraulic conductivity in cold regions and its relation to pore size and geometry. *Hydrological Processes*, *22*(15), 2829–2837. https://doi.org/10.1002/hyp.7027

Rawlins, M. A., Steele, M., Holland, M. M., Adam, J. C., Cherry, J. E., Francis, J. A., et al. (2010). Analysis of the Arctic system for freshwater cycle intensification: Observations and expectations. *Journal of Climate*, *23*(21), 5715–5737. https://doi.org/10.1175/2010JCLI3421.1

Richter, B. D., Baumgartner, J., Wigington, R., & Braun, D. (1997). How much water does a river need? *Freshwater Biology*, *37*(1), 231–249. https://doi.org/10.1046/j.1365-2427.1997.00153.x

Rovansek, R. J., Kane, D. L., & Hinzman, L. (1993). Improving estimates of snowpack water equivalent using double sampling. *Proceedings of the 61st Western Snow Conference* (pp. 157–163).

Ryan, W. A., Doesken, N. J., & Fassnacht, S. R. (2008). Evaluation of ultrasonic snow depth sensors for U.S. snow measurements. *Journal of Atmospheric and Oceanic Technology*, *25*(5), 667–684. https://doi.org/10.1175/2007jtecha947.1

Schulla, J. (2019a). Model description WaSiM-ETH. 27 August 2019. Retrieved from http://www.wasim.ch/downloads/doku/wasim/wasim_2019_en.pdf

Schulla, J. (2019b). Topographic analysis program (TANALYS). 27 August 2019. Retrieved from http://www.wasim.ch/downloads/doku/helptools/tanalys_en.pdf

Serreze, M. C., & Francis, J. A. (2006). The Arctic amplification debate. *Climatic Change*, *76*(3–4), 241–264. https://doi.org/10.1007/s10584-005-9017-y

Shiklomanov, A. I., Yakovleva, T. I., Lammers, R. B., Karasev, I. P., Vörösmarty, C. J., & Linder, E. (2006). Cold region river discharge uncertainty—Estimates from large Russian rivers. *Journal of Hydrology*, *326*(1), 231–256. https://doi.org/10.1016/j.jhydrol.2005.10.037

Stuefer, S. L., Arp, C. D., Kane, D. L., & Liljedahl, A. K. (2017). Recent extreme runoff observations from coastal Arctic watersheds in Alaska. *Water Resources Research*, *53*(11), 9145–9163. https://doi.org/10.1002/2017WR020567

Sturm, M., & Holmgren, J. (2018). An automatic snow depth probe for field validation campaigns. *Water Resources Research*, *54*(11), 9695–9701. https://doi.org/10.1029/2018wr023559

Towns, J., Cockerill, T., Dahan, M., Foster, I., Gaither, K., Grimshaw, A., et al. (2014). XSEDE: Accelerating scientific discovery. *Computing in Science & Engineering*, *16*(5), 62–74. https://doi.org/10.1109/MCSE.2014.80

Vinogradov, Y. B., Semenova, O. M., & Vinogradova, T. A. (2011). An approach to the scaling problem in hydrological modeling: The deterministic modeling hydrological system. *Hydrological Processes*, *25*(7), 1055–1073. https://doi.org/10.1002/hyp.7901

White, D. M., Prokein, P., Chambers, M. K., Lilly, M. R., & Toniolo, H. (2008). Use of synthetic aperture radar for selecting Alaskan lakes for winter water use. *Journal of the American Water Resources Association*, *44*(2), 276–284. https://doi.org/10.1111/j.1752-1688.2007.00160.x

Whitman, M. S., Arp, C. D., Jones, B. M., Morris, W., Grosse, G., Urban, F. E., & Kemnitz, R. (2011). *Developing a long-term aquatic monitoring network in a complex watershed of the Alaskan Arctic Coastal Plain, paper presented at Fourth Interagency Conference on Research in Watersheds: Observing, Studying, and Managing for Change*. USGS.

Willmott, C. J. (1981). On the validation of models. *Physical Geography*, *2*, 184–194.

Woo, M. K. (1986). Permafrost hydrology in North America. *Atmosphere-Ocean*, *24*(3), 201–234. https://doi.org/10.1080/07055900.1986.9649248

Woo, M.-K., & Guan, X. J. (2006). Hydrological connectivity and seasonal storage change of tundra ponds in a polar oasis environment, Canadian High Arctic. *Permafrost and Periglacial Processes*, *17*(4), 309–323. https://doi.org/10.1002/ppp.565

Yang, D., Goodison, B. E., Ishida, S., & Benson, C. S. (1998). Adjustment of daily precipitation data at 10 climate stations in Alaska: Application of World Meteorological Organization intercomparison results. *Water Resources Research*, *34*(2), 241–256. https://doi.org/10.1029/97WR02681

Zhang, Y., Carey, S. K., Quinton, W. L., Janowicz, J. R., Pomeroy, J. W., & Flerchinger, G. N. (2010). Comparison of algorithms and parameterizations for infiltration into organic-covered permafrost soils. *Hydrology and Earth System Sciences*, *14*(5), 729–750. https://doi.org/10.5194/hess-14-729-2010

Zhang, Z., Kane, D. L., & Hinzman, L. D. (2000). Development and application of a spatially distributed Arctic hydrological and thermal process model (ARHYTHM). *Hydrological Processes*, *14*(6), 1017–1044. https://doi.org/10.1002/(SICI)1099-1085(20000430)14:6<1017::AID-HYP982>3.0.CO;2-G